The gamma-ray Moon seen by the Fermi LAT

IOP Conf. Series: Journal of Physics: Conf. Series **934** (2017) 012021 doi:10.1088/1742-6596/934/1/012021

The gamma-ray Moon seen by the Fermi LAT

F. Loparco (on behalf of the Fermi LAT Collaboration)

Dipartimento di Fisica "M. Merlin" dell'Università e del Politecnico di Bari, I-70126 Bari, Italy
Istituto Nazionale di Fisica Nucleare, Sezione di Bari, I-70126 Bari, Italy

E-mail: francesco.loparco@ba.infn.it

Abstract. When seen in gamma rays, the Moon appears brighter than the Sun. Gamma rays emitted by the Moon mostly originate from the decays of neutral pions produced by the interactions of cosmic rays with the lunar surface. Using the data collected by the *Fermi* Large Area Telescope (LAT) in its first seven years of operation, we measured the gamma-ray emission spectrum of the Moon in the energy range from 30 MeV up to a few GeV and we studied its time evolution, finding a correlation with the solar activity. We also developed a full Monte Carlo simulation based on the FLUKA code, which describes the production of gamma rays in the cosmic-ray interactions with the Moon. We used the simulation results to infer the cosmic-ray proton and helium spectra near the Earth from the lunar gamma-ray data.

1. Introduction

High energy gamma rays emitted from the Moon are produced in the inelastic collisions of cosmic-ray nuclei (CRs) with the lunar surface. The gamma-ray flux from the Moon will be therefore sensitive to the primary CR energy spectra, to the composition of the lunar surface and to the mechanisms of hadronic interactions of CR nuclei with the lunar regolith.

2. Data selection

This analysis uses the data collected by the *Fermi* LAT [1] from August 2008 to June 2015. It has been performed using the newest Pass 8 data [2] and selecting P8_SOURCE photon events starting from a minimum energy of 30 MeV.

In our analysis we have defined a signal region as a cone centered on the Moon position and a background region as a cone centered on a time-offset Moon position. Since the Moon orbits around the Earth with a period of ~ 28 days, we chose a time offset of 14 days (i.e. at a given time, the center of the background region is in the position that the Moon will take 14 days later).

The angular radius of the two regions is given by:

$$\theta = \sqrt{[\theta_0 (E/E_0)^{-\delta}]^2 + \theta_{min}^2} \tag{1}$$

where E is the photon energy, $E_0 = 100\,\mathrm{MeV}$, $\theta_{min} = 1^\circ$, $\theta_0 = 5^\circ$ and $\delta = 0.8$. The energy dependence of the angular radius follows the behavior of the 68% containment radius of the LAT point-spread function (PSF) [3]. This choice maximizes the signal-to-noise ratio. The value of θ_{min} in Eq. 1 has been chosen to account for the finite dimension of the Moon, which is seen from the Earth as an extended source of 0.25° angular radius. The position of the Moon is

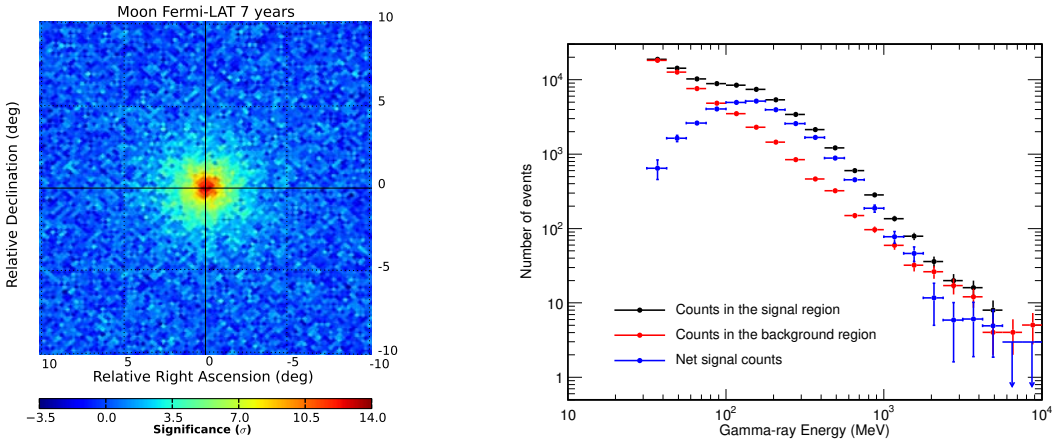

Figure 1. Left panel: significance map of the Moon as a function of right ascension and declination (the coordinates are centered on the Moon). The map is built with photons in the energy range from 30 MeV to 10 GeV. Right panel: photon count spectra in the signal (black circles) and background regions(red circles). The net signal count spectrum (blue circles) is superimposed. The plots are taken from ref. [10].

obtained from its ephemeris using a software interfaced to the JPL libraries [4] and correcting for *Fermi* orbital parallax.

For our analysis we selected the time intervals when the LAT was operating in its standard science operation configuration and was outside the South Atlantic Anomaly (SAA). To avoid contamination from the bright limb of the Earth we discarded the data taken during the times when the angular separation between a cone of angular radius $\theta_{max} = 15^\circ$ centered on the Moon direction (or on the time-offset Moon direction) and the zenith direction exceeded 100°. We also discarded data taken during the times when the center of the signal (background) region was observed with off-axis angles θ larger than 66.4° (i.e. $\cos\theta < 0.4$). Furthermore we selected only the periods where the Moon (or the time-offset Moon) was at a Galactic latitude Finally, we required a minimum angular distance of 20° between the Moon (or the time-offset Moon) and the Sun and between the Moon (or the time-offset Moon) and any celestial source in the 2FGL *Fermi* LAT source catalog [5].

The left panel of Fig. 1 shows the significance map of the Moon, evaluated with photons in the energy range from 30 MeV to 10 GeV. The sky has been divided into 786432 pixels, each one covering a solid angle of $\approx 1.6 \times 10^{-5}$ sr using the HEALPix [6] pixelization tool. The significance of each pixel has been evaluated with the formula of ref. [7], starting from the counts in the signal and in the background regions and taking into account the lifetime ratio between the two regions. A clear peak is found in the center of the map, corresponding to the gamma-ray emission from the Moon.

The right panel of Fig. 1 shows the observed photon count spectra in the signal and background regions, and the net signal count spectrum, which has been calculated by applying in each energy bin the Bayesian procedure illustrated in ref. [8], taking into account the lifetimes of the signal and background regions and assuming uniform priors for the net signal counts in each energy bin.

3. Evaluation of the gamma-ray flux from the Moon

We have reconstructed the energy spectrum of gamma rays from the Moon starting from the observed count spectra in the signal and in the background regions and using an analysis

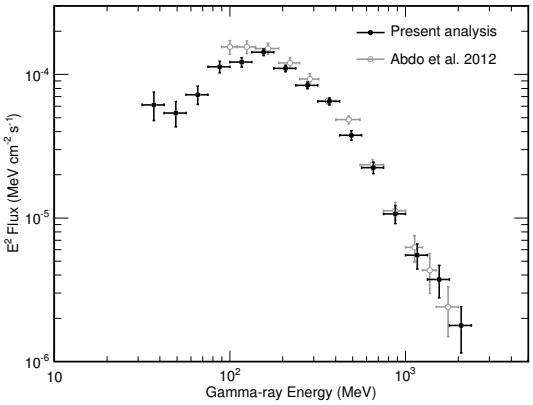

Figure 2. Gamma-ray flux from the Moon in the period from August 2008 to June 2015 compared with the results of ref. [11]. The central values of each bin represent the mean flux values, while the error bars represent the RMSs of the corresponding PDFs. The plot is taken from ref. [10].

method based on the software toolkit BAT [9], which allows to evaluate the posterior probability distribution functions (PDFs) for the parameters of a model. In our analysis we used BAT to evaluate, starting from the count spectra in the signal and background regions, the posterior PDFs for the signal and background gamma-ray fluxes in 15 energy bins. The calculation is performed by maximizing a Poisson likelihood function, in which the the expected counts are evaluated folding the fluxes with the exposure and taking energy dispersion into account. The full details of the analysis are discussed in ref. [10].

Figure 2 shows the reconstructed gamma-ray spectrum of the Moon, compared with the spectrum published in ref. [11], which was obtained from the analysis of the first 2 years of data taken by the *Fermi* LAT. At energies above 150 MeV the present results are consistent with those of ref. [11], while some discrepancies are observed at lower energies, due to the solar modulation effect on CRs. The data sample analyzed in ref. [11] was taken in the first 2 years of LAT operations, when the solar activity was at a minimum; on the other hand, the present data sample corresponds to a period of 7 years, covering more than half of a solar cycle.

4. Time evolution of the lunar gamma-ray emission

To study the time evolution of the lunar gamma-ray emission we have divided our dataset into smaller samples, each corresponding to a period of 6 months. The left panel of Fig. 3 shows the time evolution of the gamma-ray intensity from the Moon measured by the LAT above 56, 75, 100 and 178 MeV. As expected, the gamma-ray intensity from the Moon follows the evolution of the solar cycle. This feature is confirmed when looking at the correlations between the lunar gamma-ray intensity and the data from various neutron monitor stations installed in various locations on the Earth. As an example, in the right panel of Figure 3 it is shown a comparison of the lunar gamma-ray intensity measured by the LAT with the count rates of the McMurdo neutron monitor [12]. Furthermore, as the gamma-ray threshold energy is increased, the correlation with the solar cycle becomes weaker, as gamma rays of higher energies are produced by more energetic cosmic rays, which are not affected by the solar modulation.

5. Evaluation of the low-energy CR spectra and of the solar modulation potential

We have implemented a Monte Carlo simulation of the interactions of CR protons and ^{4}He nuclei with the lunar surface based on the FLUKA toolkit [13]. The Moon is described as a sphere of radius $R = 1737.1$ km, consisting of a mixture of different oxides (45% SiO_2, 22% FeO, 11% CaO, 10% Al_2O_3, 9% MgO, 3% FeO) with a density $\rho = 1.8$ g cm^{-3}.

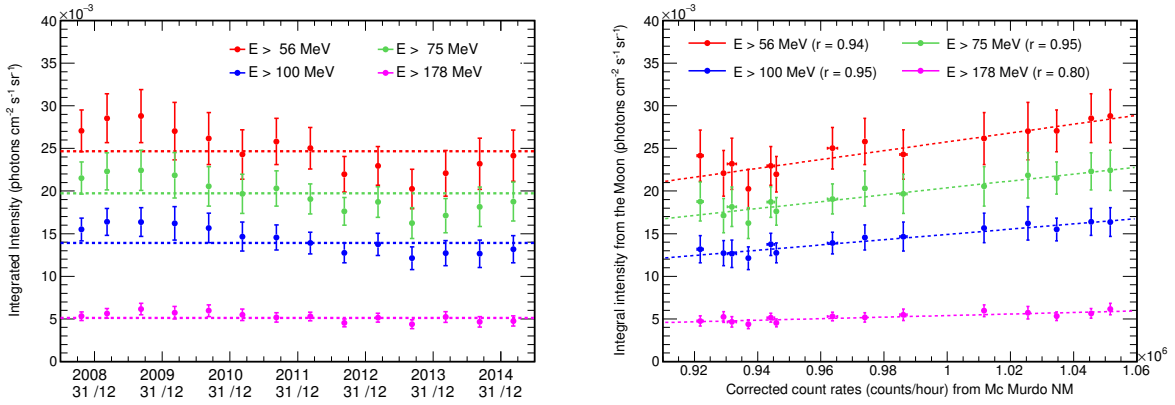

Figure 3. Left panel: Time evolution of the intensity of gamma rays emitted from the Moon above 56, 75, 100 and 178 MeV. The shaded areas indicate the average values over the whole data taking period. Right panel: Study of the correlations between the lunar gamma-ray intensity and the count rate of the McMurdo neutron monitor. The plots are taken from ref. [10].

The gamma-ray flux from the Moon can be expressed as.

$$\phi_\gamma(E_\gamma) = \frac{\pi R^2}{d^2} \sum_{i=p,He} \int Y(E_\gamma|T_i) I(T_i) dT_i \tag{2}$$

where d is the LAT-Moon distance, $I(T_i)$ is the intensity of CRs of the i-th species impinging on the Moon as a function of kinetic energy and $Y(E_\gamma|T_i)$ is the corresponding gamma-ray yield. To check our simulation, we have verified that the lunar gamma-ray flux calculated with eq. 2 using the CR proton and ^{4}He intensities measured by AMS-02 [16, 17] reproduces the LAT data taken in the same epoch.

The gamma-ray yields evaluated from the simulation have been used to fit the Moon data in order to evaluate the solar modulation potential. The fit procedure is based on BAT, and is similar to the one described in sec. 3 for the reconstruction of the gamma-ray fluxes. Here we have assumed a model for the local interstellar spectra (LIS) of CR protons and ^{4}He nuclei [14], and we have assumed that their spectra at the Solar System can be calculated from the LIS in the framework of the force field approximation [15] in terms of a single parameter, the solar modulation potential. In this analysis the parameters to be fitted are the background photon fluxes (which can be treated as nuisance parameters) and the solar modulation potential.

The fit procedure results into an average value of the solar modulation potential of (537 ± 12) MV during the whole data taking period. In the left panel of Fig. 4, the fitted gamma-ray spectrum from the Moon is compared with the measured fluxes in the individual energy bins. The fitted spectrum reproduces the data fairly well, although above 400 MeV it tends to overestimate the measured fluxes. The right panel of Fig. 4 show the modulated CR proton and ^{4}He spectra inferred from this analysis. Both the spectra are consistent with the results from direct measurements performed by PAMELA [18] and AMS-02 [16, 17].

Acknowledgments
The *Fermi* LAT Collaboration acknowledges support for LAT development, operation and data analysis from NASA and DOE (United States), CEA/Irfu and IN2P3/CNRS (France), ASI and INFN (Italy), MEXT, KEK, and JAXA (Japan), and the K.A. Wallenberg Foundation, the

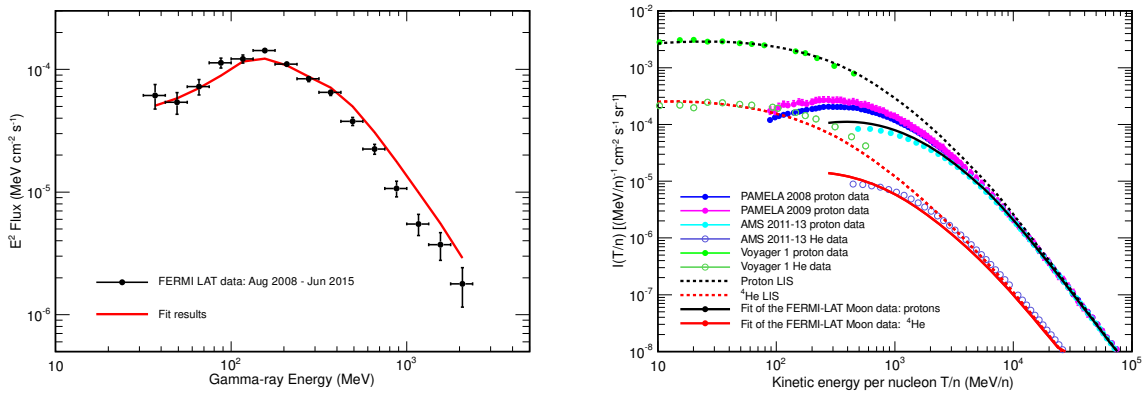

Figure 4. Left panel: gamma-ray flux from the Moon. The fitted spectrum (red line) is compared with the measured fluxes in the individual energy bins (black circles). Right panel: CR proton and ^{4}He spectra obtained from a fit of the *Fermi* LAT Moon gamma-ray data. The result is compared with the direct measurements performed by PAMELA [18] and AMS-02 [16, 17] in different epochs. The Voyager 1 proton and helium data [19] taken at ~ 120 AU from the Sun are also shown. The plots are taken from ref. [10].

Swedish Research Council and the National Space Board (Sweden). Science analysis support in the operations phase from INAF (Italy) and CNES (France) is also gratefully acknowledged. This work performed in part under DOE Contract DE-AC02-76SF00515.

References

[1] Atwood W B *et al.* 2009 *Astrophys. J.* **697** 1071
[2] Atwood W B *et al.* (Fermi-LAT Collaboration) 2013 Fermi Symposium proceedings *eConf C121028* (*Preprint* 1303.3514)
[3] http://fermi.gsfc.nasa.gov/ssc/data/analysis/documentation/Cicerone/Cicerone_LAT_IRFs/IRF_PSF.html
[4] Folkner W M *et al.* 2014 JPL Interplanetary Network Progress Report 42-196 http://ipnpr.jpl.nasa.gov/progress_report/42-196/196C.pdf
[5] Nolan P *et al.* 2012 *Astrophys. J. Supp.* **199** 31
[6] Gorski K M *et al.* 2005 *Astrophys. J.* **622** 759
[7] Li T and Ma Y 1983 *Astrophys. J.* **272** 317
[8] Loparco F and Mazziotta M N 2011 *Nucl. Inst. Meth.* A **646** 167
[9] Caldwell A, Kollar D and Krøninger K 2009 *Comput. Phys. Commun.* **180** 2197
[10] Ackermann M *et al.* 2016 *Phys. Rev.* D **93** 082001
[11] Abdo A A *et al.* *Astrophys. J.* **758** 140
[12] Home page of the University of Delaware Bartol Research Institute Neutron Monitor Program: neutronm.bartol.udel.edu
[13] http://www.fluka.org
[14] Mazziotta M N *et al.* 2016 *Astrop. Phys.* **81** 21
[15] Gleeson L J and Axford W I 1967 *Astrophys. J.* **149** L115
Gleeson L J and Axford W I 1968 *Astrophys. J.* **154** 1011
[16] Aguilar M *el al.* 2015 *Phys. Rev. Lett.* **114** 171103
[17] Aguilar M *et al.* 2015 *Phys. Rev. Lett.* **115** 211101
[18] Adriani O *et al.* 2013 *Astrophys. J.* **765** 91 (*Preprint* 1301.4108)
[19] Stone E C *et al.* 2013 *Science* **341** 150